Model Predictive Control of Nonlinear Stochastic Partial Differential Equations with Application to a Sputtering Process

Yiming Lou
Advanced Projects Research, Inc., 1925 McKinley Ave. Suite B, La Verne, CA 91750

Gangshi Hu
Dept. of Chemical and Biomolecular Engineering, University of California, Los Angeles, CA 90095

Panagiotis D. Christofides
Dept. of Electrical Engineering, University of California, Los Angeles, CA 90095

Dept. of Chemical and Biomolecular Engineering, University of California, Los Angeles, CA 90095

DOI 10.1002/aic.11511
Published online June 4, 2008 in Wiley InterScience (www.interscience.wiley.com).

A method is developed for model predictive control of nonlinear stochastic partial differential equations (PDEs) to regulate the state variance, which physically represents the roughness of a surface in a thin film growth process, to a desired level. Initially a nonlinear stochastic PDE is formulated into a system of infinite nonlinear stochastic ordinary differential equations by using Galerkin's method. A finite-dimensional approximation is then derived that captures the dominant mode contribution to the state variance. A model predictive control problem is formulated, based on the finite-dimensional approximation, so that the future state variance can be predicted in a computationally efficient way. To demonstrate the method, the model predictive controller is applied to the stochastic Kuramoto-Sivashinsky equation, and the kinetic Monte Carlo model of a sputtering process to regulate the surface roughness at a desired level. © 2008 American Institute of Chemical Engineers *AIChE J,* 54: 2065–2081, 2008
Keywords: process control, simulation, process

Introduction

The height fluctuation of thin film surfaces, which can be described by the thin film surface roughness, can significantly affect the quality of thin films, and is an important variable from a control and optimization point of view. The need to improve the quality and microstructure of thin films of advanced materials by implementing real-time feedback control in industrially important materials processes has motivated extensive research over the last five years on the development of advanced control and optimization methods for multiscale process systems using fundamental deterministic/stochastic process models (see, for example, a recent review article[1] and the references therein). Kinetic Monte Carlo (kMC) models were initially used to develop a methodology for feedback control of thin film surface roughness.[2,3] The method was successfully applied to control surface roughness in a gallium arsenide (GaAs) deposition process model,[4] and to control complex deposition processes including multiple components with both short-range and

Correspondence concerning this article should be addressed to P. Christofides at pdc@seas.ucla.edu
Current address of Y. Lou: Hamilton Sundstraud United Technologies Corporation, 2771 North Garey Avenue, Pomona, CA 91767.

long-range interactions.[5] Furthermore, a method for computationally efficient optimization of thin film growth using coupled macroscopic and microscopic models was developed.[6] However, the fact that kMC models are not available in closed-form makes it very difficult to use them for system-level analysis and the design and implementation of model-based feedback control systems. To achieve better closed-loop performance, it is desirable to design feedback controllers on the basis of closed-form process models, which account for the stochastic nature of the microscopic events. An approach was reported in[7,8,9] to identify linear deterministic models from outputs of kMC simulators and design controllers using linear control theory. This approach is effective in controlling macroscopic variables, which are low statistical moments of the microscopic distributions (e.g., surface coverage, which is the first moment of species distribution on a lattice). Other results on analysis and control of microscopic process models include the construction of reduced-order approximations of the master equation[10] and control of a coupled kMC and finite-difference simulation code of a copper electrodeposition process using empirical deterministic input-output models.[11] However, to control higher statistical moments of the microscopic distributions, such as the surface roughness (the second moment of height distribution on a lattice), or even the microscopic configuration (such as the surface morphology), deterministic models may not be sufficient, and stochastic partial differential equation (PDE) models may be needed.

Stochastic PDEs arise naturally in the modeling of the evolution of the surface height profile of ultra thin films in a variety of material preparation processes, such as thin film growth[12–15] and ion sputtering processes.[16,17] Recently, it was demonstrated that covariance control methods can be applied to stochastic PDEs and result in successful control of microscopic thin film morphology.[18,19] Specifically, a method for feedback control of surface roughness based on linear stochastic PDE process models was developed in.[19,18] This method involves reformulation of the linear stochastic PDE into a system of infinite linear stochastic ordinary differential equations (ODEs) by using modal decomposition, derivation of a finite-dimensional approximation that captures the dominant mode contribution to the surface roughness, and state feedback controller design based on the finite-dimensional approximation. Furthermore, a systematic identification approach was developed for linear stochastic PDEs,[18] and a method for construction of linear stochastic PDE models for thin film growth using first principles-based microscopic simulations was developed and applied to construct linear stochastic PDE models for thin film deposition processes in two-dimensional (2-D) lattices.[20,21]

While linear control techniques work well for many applications, nonlinearities exist in many material preparation processes in which surface evolution can be modeled by stochastic PDEs. Typical examples of such processes include the sputtering process whose surface height evolution can be described by the nonlinear stochastic Kuramoto-Sivashinsky equation (KSE)[16,17] and thin film growth processes described by nonlinear stochastic PDEs.[14] To incorporate the inherent nonlinearities into the feedback controller design, we recently developed a method for nonlinear control of surface roughness using nonlinear stochastic PDEs.[22] The nonlinear controller was successfully applied to both the nonlinear stochastic KSE model and the kMC model of an ion-sputtering process to regulate the surface roughness to a desired level. However, this nonlinear controller is not optimal with respect to a meaningful cost that includes penalty on the control action.

Model predictive control (MPC) is widely used in chemical process control due to its capability to handle input and state constraints, to tolerate model uncertainty and suppress external disturbances, and to force the closed-loop system to follow a target trajectory using optimal control action (see References[23–26] for surveys of results and references in this area). In MPC, the control action is obtained by solving repeatedly, online, a finite horizon constrained open-loop optimal control problem. Recent efforts on predictive control of distributed parameter systems have focused on predictive control of deterministic parabolic PDEs, including linear systems with distributed[27] and boundary[28] control and nonlinear systems with distributed control.[29] However, results on predictive control of stochastic distributed parameter systems, to the best of our knowledge, are not available.

In this work, a method for model predictive control of nonlinear stochastic PDEs is developed. The control objective is to regulate the state variance of the PDE, e.g., the roughness of a surface in a thin film growth process, to a desired level. To present this method, a nonlinear stochastic PDE is first formulated into a infinite-dimensional nonlinear stochastic ODE system by using Galerkin's method. A finite-dimensional approximation is then constructed to capture the dominant mode contribution to the state variance. A model predictive control problem is formulated based on the finite-dimensional approximation. In the closed-loop system under the model predictive control, the control action is computed by minimizing an objective cost function, which includes both transient and terminal state penalty. An analysis of the closed-loop nonlinear infinite-dimensional system is performed to characterize the closed-loop performance enforced by the model predictive controller. Subsequently, numerical simulations are performed using the stochastic KSE to demonstrate the effectiveness of the proposed predictive controller. In addition, we consider the problem of surface roughness regulation in a 1-D ion-sputtering process described by a kMC model. We first demonstrate that the spatially distributed control configuration is more effective for surface roughness regulation compared to the spatially invariant control configuration. Then, a model predictive controller, which is designed based on an identified stochastic KSE surface model, is applied to the kMC model of the sputtering process, and is demonstrated to successfully regulate the expected surface roughness to a desired level.

Nonlinear Model Predictive Controller Design

Preliminaries

We consider nonlinear dissipative stochastic PDEs with distributed control of the following form

$$\frac{\partial h}{\partial t} = \mathcal{A}h + \mathcal{F}(h) + \sum_{i=1}^{p} b_i(x)u_i(t) + \xi(x,t) \qquad (1)$$

subject to homogeneous boundary conditions, and the initial condition $h(x, 0) = h_0(x)$, where $x \in [-\pi, \pi]$ is the spatial coordinate, t is the time, $h(x, t)$ is the height of the surface at position x and time t, $\mathcal{A}$ is a dissipative spatial differential operator, $\mathcal{F}$ is a nonlinear function, $u_i(t)$ is the i^{th} manipulated input, p is the number of manipulated inputs, and $b_i(x)$ is the i^{th} actuator distribution function (i.e., $b_i(x)$ determines how the control action computed by the i^{th} control actuator, $u_i(t)$, is distributed (e.g., point or distributed actuation) in the spatial interval $[-\pi, \pi]$). $\xi(x, t)$ is a Gaussian white noise with the following expressions for its mean and covariance

$$\begin{aligned} \langle \xi(x,t) \rangle &= 0 \\ \langle \xi(x,t)\xi(x',t') \rangle &= \sigma^2 \delta(x-x')\delta(t-t') \end{aligned} \tag{2}$$

where σ is a real number, $\delta(\cdot)$ is the Dirac delta function, and $\langle \cdot \rangle$ denotes the expected value. Note that although $\langle \cdot \rangle$ is used to denote the expected value in literature (see, for example,[14,17,30,31]), an alternative notation $E(\cdot)$, is also commonly used (see, for example,[32,33]). Throughout this work, we use $\langle \cdot \rangle$ for the expected value.

The eigenvalue problem for $\mathcal{A}$ is defined as

$$\mathcal{A}\phi_j = \lambda_j \phi_j, \quad j = 1, 2, \cdots, \infty \tag{3}$$

where λ_j and ϕ_j denote the jth eigenvalue and eigenfunction, respectively. To simplify our development and motivated by most practical applications, we consider stochastic PDEs for which $\mathcal{A}$ is a highly dissipative operator (i.e., a second-order or fourth-order linear self-adjoint operator) and has eigenvalues, which are real numbers. The eigenspectrum of $\mathcal{A}$, $\sigma(\mathcal{A})$, is defined as the set of all eigenvalues of $\mathcal{A}$, i.e., $\sigma(\mathcal{A}) = \{\lambda_1, \lambda_2, \cdots\}$. Assumption 1 states that the eigenspectrum of $\mathcal{A}$ can be partitioned into a finite-dimensional part consisting of m slow eigenvalues and a stable infinite-dimensional complement containing the remaining fast eigenvalues, the separation between the slow and fast eigenvalues of $\mathcal{A}$ is large, and that the infinite sum of $\sum_{i=1}^{\infty} \frac{1}{|\lambda_i|}$ converges to a finite positive number.

Assumption 1[34]: *The eigenvalues of $\mathcal{A}$ satisfy the following:*

1 $\lambda_1 \geq \lambda_2 \geq \cdots$.

2 $\sigma(\mathcal{A})$ *can be partitioned as* $\sigma(\mathcal{A}) = \sigma_1(\mathcal{A}) + \sigma_2(\mathcal{A})$, *where* $\sigma_1(\mathcal{A})$ *consists of the first m (with m finite) eigenvalues, i.e.,* $\sigma_1(\mathcal{A}) = \{\lambda_1, \lambda_2, \cdots, \lambda_m\}$. $\lambda_{m+1} < 0$ *and* $\frac{|\lambda_1|}{|\lambda_{m+1}|} = O(\varepsilon)$ *where* $\varepsilon < 1$ *is a small positive number.*

3 *There exists a positive number,* $\gamma > 0$, *such that* $\sum_{i=1}^{\infty} \frac{1}{|\lambda_i|} < \gamma$.

Note that the eigenvalue problem of the stochastic PDE of Eq. 1 is formulated in the same way as that of deterministic PDEs. The assumption of finite number of unstable eigenvalues and discrete eigenspectrum are always satisfied for parabolic PDE systems defined in finite spatial domains,[35] while the assumption of existence of only a few dominant modes that capture the dominant dynamics of the stochastic parabolic PDE system, and the convergence of the infinite sum $\sum_{i=1}^{\infty} \frac{1}{|\lambda_i|}$ to a finite positive number are usually satisfied by the majority of materials processes (see the example of the sputtering process described by the stochastic Kuramoto-Sivashinsky equation in the Simulation section).

The inner product and norm in the Hilbert space $\mathcal{H}$ are defined as

$$(\omega_1, \omega_2) = \int_{\Omega} (\omega_1(z), \omega_2(z))_{\mathbb{R}^n} dz, \quad \|\omega_1\|_2 = (\omega_1, \omega_2)^{1/2} \tag{4}$$

where ω_1, ω_2 are two elements of $\mathcal{H}$, Ω is the domain of definition of the process, and the notation $(\cdot, \cdot)_{\mathbb{R}^n}$ denotes the standard inner product in $\mathbb{R}^n$.

Model reduction

We apply Galerkin's method (see[35] for a detailed discussion on the standard Galerkin's method) to the system of Eq. 1 to derive an approximate finite-dimensional system. First, the solution of Eq. 1 is expanded into an infinite series in terms of the eigenfunctions of the operator of Eq. 3 as follows

$$h(x,t) = \sum_{n=1}^{\infty} \alpha_n(t)\phi_n(x) \tag{5}$$

where $\alpha_n(t)$ are time-varying coefficients. Substituting the above expansion for the solution $h(x, t)$, into Eq. 1, and taking the inner product with the adjoint eigenfunctions $\phi_n^*(x)$, the following system of infinite nonlinear stochastic ODEs is obtained

$$\frac{d\alpha_n}{dt} = \lambda_n \alpha_n + f_{n\alpha} + \sum_{i=1}^{p} b_{i\alpha_n} u_i(t) + \xi_{\alpha}^n(t), \quad n = 1, \ldots, \infty \tag{6}$$

where

$$b_{i\alpha_n} = \int_{-\pi}^{\pi} \phi_n^*(x) b_i(x) dx, \quad \xi_{\alpha}^n(t) = \int_{-\pi}^{\pi} \xi(x,t)\phi_n^*(x) dx \tag{7}$$

and

$$f_{n\alpha} = \int_{-\pi}^{\pi} \phi_n^*(x) \mathcal{F}(h) dx \tag{8}$$

The covariances of $\xi_{\alpha}^n(t)$ can be computed by using the following result:

Result 1: If (1) $f(x)$ is a deterministic function, (2) $\eta(x)$ is a random variable with $\langle \eta(x) \rangle = 0$ and covariance $\langle \eta(x)\eta(x') \rangle = \sigma^2 \delta(x-x')$, and (3) $\varepsilon = \int_a^b f(x)\eta(x)dx$, then ε is a real random number with $\langle \varepsilon \rangle = 0$ and covariance $\langle \varepsilon^2 \rangle = \sigma^2 \int_a^b f^2(x)dx$.[36]

Using Result 1, the covariance of $\xi_{\alpha}^n(t)$ can be obtained as $\langle \xi_{\alpha}^n(t)\xi_{\alpha}^n(t') \rangle = \sigma^2 \delta(t-t')$.

Owing to its infinite-dimensional nature, the system of Eq. 6 cannot be directly used for the design of controllers that can be implemented in practice (i.e., the practical implementation of controllers which are designed on the basis of this system will require the computation of infinite sums which cannot be done by a computer). Instead, we will base the controller design on a finite-dimensional approximation of this system. Subsequently, we will show that the resulting controller will enforce the desired control objective in the closed-loop infinite-dimensional system. Specifically, we rewrite the system of Eq. 6 as follows

$$\begin{aligned} \frac{dx_s}{dt} &= \mathcal{A}_s x_s + \mathcal{F}_s(x_s, x_f) + \mathcal{B}_s u + \xi_s \\ \frac{dx_f}{dt} &= \mathcal{A}_f x_f + \mathcal{F}_f(x_s, x_f) + \mathcal{B}_f u + \xi_f \end{aligned} \tag{9}$$

where $x_s = [\alpha_1\ \alpha_2\ \cdots\ \alpha_m]^T$, $x_f = [\alpha_{m+1}\ \alpha_{m+2}\ \cdots]^T$, $\mathcal{A}_s = diag[\lambda_1\ \lambda_2\ \cdots\ \lambda_m]$, $\mathcal{A}_f = diag[\lambda_{m+1}\ \lambda_{m+2}\ \cdots]$, $\mathcal{F}_s(x_s, x_f) = [f_{1\alpha}(x_s,x_f)\ f_{2\alpha}(x_s, x_f)\ \cdots\ f_{m\alpha}(x_s, x_f)]^T$, $\mathcal{F}_f(x_s, x_f) = [f_{m+1\alpha}(x_s, x_f)\ f_{m+2\alpha}(x_s, x_f)\ \cdots]^T$, $u = [u_1\ u_2\ \cdots\ u_p]$, $\xi_s = [\xi_\alpha^1\ \cdots\ \xi_\alpha^m]$, and $\xi_f = [\xi_\alpha^{m+1}\ \xi_\alpha^{m+2}\ \cdots]$,

$$\mathcal{B}_s = \begin{bmatrix} b_{1_{\alpha_1}} & \cdots & b_{p_{\alpha_1}} \\ \vdots & \ddots & \vdots \\ b_{1_{\alpha_m}} & \cdots & b_{p_{\alpha_m}} \end{bmatrix}, \quad \mathcal{B}_f = \begin{bmatrix} b_{1_{\alpha_{m+1}}} & \cdots & b_{p_{\alpha_{m+1}}} \\ b_{1_{\alpha_{m+2}}} & \cdots & b_{p_{\alpha_{m+2}}} \\ \vdots & \vdots & \vdots \end{bmatrix} \tag{10}$$

The standard Galerkin's method is to approximate the solution $h(x, t)$ of the system of Eq. 1 by $\tilde{x}_s(t)$, which is given by the following m–dimensional system

$$\frac{d\tilde{x}_s}{dt} = \mathcal{A}_s\tilde{x}_s + \mathcal{F}_s(\tilde{x}_s, 0) + \mathcal{B}_s u + \xi_s \tag{11}$$

where the tilde symbol in $\tilde{x}_s$ denotes that this state variable is associated with a finite-dimensional system. We note that there are a variety of other methods/concepts available for model reduction of nonlinear distributed parameter systems. For example, the concept of approximate inertial manifolds[34,35,37] can be employed to obtain improved approximations of the finite-dimensional system of Eq. 11, and proper orthogonal decomposition (POD)[38,37] can be used to derive empirical eigenfunctions based on process model solutions, which can be employed as basis functions in Galerkin's method.

Model predictive controller design

In this section, we design a nonlinear model predictive controller based on the finite-dimensional stochastic ODE system of Eq. 11. In our development, we will need the following notation for the full state $X = [x_s^T\ x_f^T]^T = [\alpha_1\ \alpha_2\ \cdots\ \alpha_m\ \alpha_{m+1}\ \cdots]^T$. The variances of x_s, x_f and X are defined as

$$\begin{aligned} var(x_s(t)) &= \left[\left\langle \alpha_1(t)^2 \right\rangle \quad \cdots \quad \left\langle \alpha_m(t)^2 \right\rangle\right]^T \\ var(x_f(t)) &= \left[\left\langle \alpha_{m+1}(t)^2 \right\rangle \quad \left\langle \alpha_{m+2}(t)^2 \right\rangle \quad \cdots\right]^T \\ var(X(t)) &= \left[var(x_s(t))^T \quad var(x_f(t))^T\right]^T \end{aligned} \tag{12}$$

where $\langle\cdot\rangle$ denotes the expected value. The 2-norms of a finite-dimensional vector $y_s(t) = [y_1(t)\ y_2(t)\ \cdots\ y_m(t)]^T$ and an infinite-dimensional vector $y_f(t) = [y_1(t)\ y_2(t)\ \cdots]^T$ are defined as follows

$$\begin{aligned} \|y_s(t)\| &= \sqrt{\sum_{j=1}^{m} y_j(t)^2} \\ \left\|y_f(t)\right\| &= \sqrt{\sum_{j=1}^{\infty} y_j(t)^2} \end{aligned} \tag{13}$$

Accordingly, we have the following for the norms of the vectors $var(x_s)$, $var(x_f)$ and $var(X)$

$$\begin{aligned} \|var(x_s(t))\|^2 &= \sum_{j=1}^{m} \left\langle \alpha_j(t)^2 \right\rangle^2 \\ \left\|var(x_f(t))\right\|^2 &= \sum_{j=m+1}^{\infty} \left\langle \alpha_j(t)^2 \right\rangle^2 \\ \|var(X(t))\|^2 &= \sum_{j=1}^{\infty} \left\langle \alpha_j(t)^2 \right\rangle^2 \end{aligned} \tag{14}$$

MPC formulation based on the infinite-dimensional system

In this section, we consider the problem of control of the norm of the state variance of the nonlinear stochastic infinite-dimensional system of Eq. 1 to a desired level. This problem will be addressed within a model predictive control framework, where the control, at a time t and state $x(t)$, is obtained by solving a finite-horizon optimal control problem. Since the system of infinite stochastic ODEs of Eq. 9 is mathematically equivalent to the stochastic PDE of Eq. 1, the MPC problem is formulated based on the system of infinite stochastic ODEs of Eq. 9 in the following form

$$\begin{aligned} \min_u \quad & \{J(X(t), t, u(\cdot))|u(\cdot) \in S\} \\ s.t \quad & \\ & \frac{dx_s}{dt} = \mathcal{A}_s x_s + \mathcal{F}_s(x_s, x_f) + \mathcal{B}_s u + \xi_s \\ & \frac{dx_f}{dt} = \mathcal{A}_f x_f + \mathcal{F}_f(x_s, x_f) + \mathcal{B}_f u + \xi_f \end{aligned} \tag{15}$$

where $S = S(t, T_p)$ is the family of piecewise functions, with period Δ, mapping $[t,t + T_p]$ into $u = \{u(t) \in \mathbb{R}^l\}$ and T_p is a specified prediction horizon. The control $u(\cdot)$ in S is characterized by the sequence $u[k]$, where $u[k] = u(t+k\Delta)$ and satisfies that $u(t) = u[k]$ for all $t \in [t+k\Delta,\ t+(k+1)\Delta]$. Note that by selecting an appropriate S, input constraints can be readily included in the control problem formulation. The objective function $J(X(t), t, u(\cdot))$ is, in general, given by

$$\begin{aligned} J(X, t, u(\cdot)) = \int_t^{t+T_p} & Q\|var(X^u(\tau)) - var(X^*(\tau))\|^2 d\tau \\ & + Q_f\left\|var(X(t+T_p)) - var(X^*(t+T_p))\right\|^2 \end{aligned} \tag{16}$$

where $var(X^*(\tau))$ is the reference trajectory describing the variance of the desired state for the infinite-dimensional system, $var(X^u(\tau))$ denotes the variance of the state X that is due to the control $u(t)$, with initial state $X(t)$ at a time t in the closed-loop system of Eq. 1, Q and Q_f are positive real numbers, and T_p is the prediction horizon. We note that the cost function of Eq. 16 does not include a penalty on the control action. Yet, we do impose an implicit penalty on the control action by imposing appropriate bounds on the eigenvalues of the closed-loop system (see optimization formulation of Eq. 21 below). The minimizing control $u^0(\cdot) = \{u(t),\ u(t + \Delta),\ u(t + 2\Delta),\ \ldots\} \in S$ is then applied to the system over the interval $[t,\ t + \Delta]$, and the procedure is repeated at $t + \Delta$ until a terminal time is reached. This defines an implicit model predictive control law as follows

$$u(t) = M(X(t)) = u^0(\Delta; X(t), t) \tag{17}$$

in which $M(x(t))$ denotes the nonlinear map between the state and control.

MPC formulation and solution based on the reduced-order model

Note that the predictive control formulation shown in Eq. 15 is developed on the basis of an infinite-dimensional stochastic system. Therefore, it leads to a predictive controller that is of infinite order and cannot be realized in practice. To address this issue, we provide a predictive control formulation that is on the basis of the finite-dimensional system of Eq. 11, and computes the control action by minimizing an objective function including the distance between the predicted state variance and a reference trajectory and a terminal penalty.

Consider a vector of reference trajectories describing the desired trajectories for each element of the variance of x_s, $var(x_s^*(t)) = [\langle x_1^*(t)^2\rangle \ \cdots \ \langle x_m^*(t)^2\rangle]^T$. The control action $u(t)$, can be obtained by solving, in a receding horizon fashion, the following optimization problem

$$\begin{aligned}\min_{u} \quad & \int_t^{t+T_p} Q\left\|var(\tilde{x}_s^u(\tau)) - var(x_s^*(\tau))\right\|^2 d\tau \\ & + Q_f\left\|var(\tilde{x}_s^u(t+T_p)) - var(x_s^*(t+T_p))\right\|^2 \\ s.t \quad & \frac{d\tilde{x}_s}{dt} = \mathcal{A}_s\tilde{x}_s + \mathcal{F}_s(\tilde{x}_s,0) + \mathcal{B}_s u + \xi_s \end{aligned} \tag{18}$$

where $\tilde{x}_s^u(\tau)$ is the solution of Eq. 11 that is due to the control $u(\tau)$, with an initial condition $\tilde{x}_s(t)$ at a time t.

A challenge for the design of a predictive controller for a stochastic process is to predict the state variance $var(x_s(t))$, in a computationally efficient way. Although, a realization of the future evolution of state variance can be solved through numerical integrations of the stochastic process model of Eq. 18, due to the stochastic nature of the process, numerical solutions from different simulation runs of the same stochastic process are not identical. The state variance should be computed by averaging the numerical solutions of the stochastic process from a large number of individual simulation runs. The prediction of state variance using brute force numerical integration of a nonlinear stochastic system is, therefore, extremely computationally expensive, and is not appropriate for the design of predictive controllers to be implemented in real-time.

As an alternative, an analytical solution of the state variance based on the process model, if available, provides a feasible way for MPC design and implementation. For linear stochastic PDEs, the analytical solution of the state variance is readily available, which results in efficient design of a model predictive controller for surface variance regulation.[21] However, analytical solutions of the state variance for nonlinear stochastic PDEs are, in general, not available. To this end, we focus on the construction of a nonlinear feedback controller that can induce a linear structure in the closed-loop finite-dimensional stochastic system of Eq. 11. Therefore, the analytical solution of the state variance under the proposed controller structure can be obtained. Consequently, the control action is computed by solving an optimization problem in a receding horizon fashion and computationally efficient way.

Specifically, under the assumption that the number of control actuators is equal to the dimension of the $\tilde{x}_s$-subsystem and the matrix B_s is invertible, the control law takes the following form

$$u(t) = \mathcal{B}_s^{-1}\{(\mathcal{A}_{cs}(t) - \mathcal{A}_s)\tilde{x}_s(t) - \mathcal{F}_s(\tilde{x}_s(t),0)\} \tag{19}$$

where $\mathcal{A}_{cs}(t) = diag[\lambda_{c1}(t) \ \cdots \ \lambda_{cm}(t)]$, ($\lambda_{ci}(t)$, $i = 1, 2, \ldots, m$ are time-varying, desired poles of the closed-loop finite-dimensional system). Note that in the proposed controller structure of Eq. 19, the desired poles are not fixed values, but will be computed in real-time by solving an online optimization problem in a receding horizon fashion. This is a fundamental difference from the nonlinear feedback controller proposed in our previous work.[22]

Replacing the u of Eq. 11 by Eq. 19, we have the following closed-loop system

$$\frac{d\tilde{x}_s(t)}{dt} = \mathcal{A}_{cs}(t)\tilde{x}_s(t) + \xi_s \tag{20}$$

In this control problem formulation, the computation of the control action $u(t)$, is equivalent to the computation of $\mathcal{A}_{cs}(t)$, or the values of $\lambda_{ci}(t)$ for $i = 1, 2, \ldots, m$, by solving the following optimization problem

$$\begin{aligned}\min_{\mathcal{A}_{cs}(t)} \quad & \int_t^{t+T_p} \left(Q\left\|var(\tilde{x}_s(\tau)) - var(x_s^*(\tau))\right\|^2\right) d\tau \\ & + Q_f\left\|var(\tilde{x}_s(t+T_p)) - var(x_s^*(t+T_p))\right\|^2 \\ s.t \quad & \frac{d\tilde{x}_s}{dt} = \mathcal{A}_{cs}(t)\tilde{x}_s + \xi_s \\ & a_i < \lambda_{ci}(t) < b_i < 0; \quad i = 1,2,\ldots,m \end{aligned} \tag{21}$$

Note that in the optimization problem of Eq. 21, $\mathcal{A}_{cs}(t)$ does not change during the optimization time interval $t < \tau < t + T_p$. Therefore, the optimization problem of Eq. 21, which does not include penalty on the control action, is a quadratic problem with linear constraints for which the existence of the optimal solution is guaranteed and unique. The control action u, is computed using Eq. 19, in which $\mathcal{A}_{cs}(t)$ is obtained from the solution of the constrained optimization problem of Eq. 21. Since the poles of the closed-loop finite dimensional system $\lambda_{ci}(t)$, are constrained, u is not explicitly included in the objective function. The analytical solution of the state variance of Eq. 20 can be obtained as follows

$$\tilde{x}_n(\tau) = e^{\lambda_{cn}(\tau-t)}\tilde{x}_n(t) + \int_t^{\tau} e^{\lambda_{cn}(t+T_p-\mu)}\xi_s^n(\mu)d\mu; \quad n = 1,2,\ldots,m \tag{22}$$

The expected value (the first stochastic moment), and the variance (the second stochastic moment) of the state of Eq. 20 can be computed as follows[18,21]

$$\begin{aligned}\langle\tilde{x}_n(\tau)\rangle &= e^{\lambda_{cn}(\tau-t)}\tilde{x}_n(t) \\ \left\langle\tilde{x}_n(\tau)^2\right\rangle &= \frac{e^{2\cdot\lambda_{cn}(\tau-t)}-1}{2\cdot\lambda_{cn}} + \langle\tilde{x}_n(t)\rangle^2; \quad n = 1,2,\ldots,m \end{aligned} \tag{23}$$

Equation 23 gives the analytical solution of $var(\tilde{x}_s(t))$ in the closed-loop finite-dimensional system of Eq. 11. Using Eq. 23, the optimization problem of Eq. 21 can be subsequently formulated as a minimization of a nonlinear algebraic equation, which can be readily solved by using standard unconstrained or constrained multidimensional nonlinear minimization algorithms (for example, Nelder-Mead method or golden section search[39,40]). The computational cost of these optimization algorithms grows with the number of variables and the computation involves only standard numerical operations, such as function evaluation and comparison. The optimization problems can be solved fast relative to the time scale of process evolution using currently available computing power.

Remark 1 *Note that input and state constraints could be incorporated into the predictive control formulation of Eq. 18. In a stochastic process, the value of either the input or the state at a specific time is not predictable, and its evolution can only be described by its statistical moments. Therefore, the state constraints should be incorporated into the predictive control formulation in the form of their statistical moments. Of particular interest are their second-order moments (covariance), because the state covariance represents the expected surface roughness of a thin film,[18,19] and the input covariance can be related to control energy.[41] However, systematic handling of input and/or state constraints in predictive control of stochastic PDEs also requires an efficient way to compute the state and/or input covariance, which is, in general, very challenging for nonlinear stochastic PDEs and is outside of the scope of this work.*

Analysis of the closed-loop infinite-dimensional system

In this section, we analyze the state variance of the infinite dimensional system under the predictive controller of Eq. 21. To ensure exponential stability of the closed-loop finite-dimensional system, the upper-bounds of the closed-loop poles in Eq. 21, b_i, $i = 1, 2, \ldots, m$, are all negative. Under this condition, a Lyapunov function can be constructed to prove the exponential stability of the closed-loop finite-dimensional system with time-varying matrix $\mathcal{A}_{cs}(t)$ in Eq. 21 (note that $\mathcal{A}_{cs}(t)$ is a diagonal matrix). To this end, we can design the predictive controller of Eq. 21 to successfully drive the variance of $\tilde{x}_s$ of the system of Eq. 20 to the desired value, e.g., $\|var(x_s(t))\|^2 = \left\|var(x_s^*(t))\right\|^2$. By applying the controller of Eqs. 19 and 21 to the infinite-dimensional system of Eq. 9, and using that $\varepsilon = \frac{|\lambda_1|}{|\lambda_{m+1}|}$, the closed-loop system takes the form

$$\begin{aligned} \frac{dx_s}{dt} &= \mathcal{A}_{cs}x_s + (\mathcal{F}_s(x_s,x_f) - \mathcal{F}_s(x_s,0)) + \xi_s \\ \varepsilon\frac{dx_f}{dt} &= \mathcal{A}_{f\varepsilon}x_f + \varepsilon\mathcal{B}_f\mathcal{B}_s^{-1}(\mathcal{A}_{cs} - \mathcal{A}_s)\tilde{x}_s \\ &\quad + \varepsilon\mathcal{F}_f(x_s,x_f) - \varepsilon\mathcal{B}_f\mathcal{B}_s^{-1}\mathcal{F}_s(\tilde{x}_s,0) + \varepsilon\xi_f \end{aligned} \tag{24}$$

where λ_1 and λ_{m+1} are the first, and the $(m + 1)$th eigenvalues of the linear operator in Eq. 9, and $\mathcal{A}_{f\varepsilon} = diag[\lambda_{\varepsilon 1}\ \lambda_{\varepsilon 2}\ \cdots]$ is an infinite-dimensional matrix defined as $\mathcal{A}_{f\varepsilon} = \varepsilon \cdot \mathcal{A}_f$.

We now proceed to characterize the accuracy with which the variance of $x = [x_s^T\ x_f^T]^T$ is controlled in the closed-loop infinite-dimensional system. Theorem 1 provides estimates of the variances of x_s and x_f of the closed-loop system of Eq. 24, and a characterization of the variance of x enforced by the controller of Eqs. 19 and 21 in the closed-loop infinite dimensional system. The proof of Theorem 1 is given in the following.

Theorem 1 *Consider the closed-loop stochastic infinite-dimensional system of Eq. 24, and the definition of* $\|var(x_s)\|^2$, $\left\|var(x_f)\right\|^2$, and $\|var(X)\|^2$ *shown in Eq. 14. Then, there exist* $\mu^* > 0$ *and* $\varepsilon^* > 0$ *such that if* $\left\|x_{f0}\right\| + \|x_{s0}\| \le \mu^*$ and $\varepsilon \in (0,\varepsilon^*]$, $\left\|var(x_s(t_f))\right\|^2$, $\left\|var(x_f(t_f))\right\|^2$, *and* $\left\|var(x(t_f))\right\|^2$ *satisfy*

$$\left\|var(x_f(t))\right\|^2 = O(\varepsilon) \tag{25}$$

$$\|var(x_s(t))\|^2 = \left\|var(x_s^*(t))\right\|^2 + O(\sqrt{\varepsilon}) \tag{26}$$

$$\|var(X(t))\|^2 = \left\|var(x_s^*(t))\right\|^2 + O(\sqrt{\varepsilon}) \tag{27}$$

where x_{f0} *and* x_{s0} *are the initial conditions for* x_f *and* x_s *in Eq. 24, respectively.*

Proof of Theorem 1. The proof of Theorem 1 includes several steps. First, we prove that the closed-loop infinite-dimensional system is asymptotically stable for a sufficiently small ε. Second, we compute the $\left\|var(x_f)\right\|^2$ using the x_f subsystem of Eq. 24, and prove Eq. 25 in Theorem 1. Then, we compute $\|var(x_s)\|^2$ using the x_s subsystem of Eq. 24, and prove Eq. 26 in Theorem 1. Finally, the proof of Theorem 1 is completed by proving Eq. 27, based on the results in Eqs. 25 and 26.

Closed-loop infinite-dimensional system stability. Let $u(t) = M(x_s)$ be the general expression of the control law corresponding to the predictive control formulation of Eq. 18. The infinite-dimensional closed-loop system of Eq. 24 can be rewritten as follows

$$\begin{aligned} \frac{dx_s}{dt} &= \mathcal{A}_s x_s + \mathcal{F}_s(x_s,x_f) + \mathcal{B}_s M(x_s) + \xi_s \\ \varepsilon\frac{dx_f}{dt} &= \mathcal{A}_{f\varepsilon}x_f + \varepsilon\mathcal{F}_f(x_s,x_f) + \varepsilon\mathcal{B}_f M(x_s) + \varepsilon\xi_f \end{aligned} \tag{28}$$

where x_f subsystem is a fast subsystem due to the eigenspectrum of $\mathcal{A}_{f\varepsilon}$. Rewriting the system of Eq. 28 in the fast-time-scale $\tau = t/\varepsilon$, and setting $\varepsilon = 0$, the x_f subsystem of Eq. 28 takes the form

$$\frac{d\bar{x}_f}{d\tau} = \mathcal{A}_{f\varepsilon}\bar{x}_f \tag{29}$$

where $\bar{x}_f$ denotes the state of the x_f subsystem after neglecting the three terms. According to Assumption 1 for the eigenspectrum of the linear operator $\mathcal{A}$, all eigenvalues of $\mathcal{A}_{f\varepsilon}$ have negative real parts. Thus, the system of Eq. 29 is exponentially stable. Setting $\varepsilon = 0$ in the system of Eq. 28, the following closed-loop finite-dimensional system is obtained

$$\begin{aligned} \frac{d\tilde{x}_s}{d\tau} &= \mathcal{A}_s\tilde{x}_s + \mathcal{F}_s(\tilde{x}_s,0) + \mathcal{B}_s M(\tilde{x}_s) + \xi_s \\ &= \mathcal{A}_{cs}\tilde{x}_s + \xi_s \end{aligned} \tag{30}$$

which is locally exponentially stable by the design of the predictive controller of Eq. 21. Therefore, there exists a positive

real number $\hat{\varepsilon}$ such that $\forall \varepsilon \in (0, \hat{\varepsilon}]$ the zero solution of the closed-loop infinite-dimensional system of Eq. 24 is locally asymptotically stable.

Proof of Eq. 25 in Theorem 1. Consider the closed-loop system of Eq. 24, and note that the terms in the right-hand-side of the x_f subsystem constitute an $O(\varepsilon)$ approximation to the term $\mathcal{A}_{f\varepsilon}x_f$. Consider also the following linear stochastic system

$$\varepsilon \frac{d\bar{x}_f}{dt} = \mathcal{A}_{f\varepsilon}\bar{x}_f + \varepsilon\xi_f \tag{31}$$

Following a similar approach to the one employed in the proof of Theorem A.1 in[42] (Kokotovic, Khalil, and O'Reilly, Academic Press; 1986) p. 361, we have that there exists an $\hat{\varepsilon}^* > 0$, such that for all $\varepsilon \in (0, \hat{\varepsilon}^*]$, we have that

$$x_f(t) = \bar{x}_f(t) + O(\sqrt{\varepsilon}) \tag{32}$$

Based on the definition of $\|var(x_f)\|^2$ in Eq. 14, we have the following estimate for $\|var(x_f(t))\|^2$.

$$\begin{aligned}&\|var(x_f(t))\|^2 \\ &\quad = \|var(\bar{x}_f(t) + O(\sqrt{\varepsilon}))\|^2 \le 2\|var(\bar{x}_f(f))\|^2 + O(\varepsilon)\end{aligned} \tag{33}$$

Furthermore, $\|var(x_f(t))\|^2$ and $\|var(\bar{x}_f(t))\|^2$ are equal to the traces of the covariance matrices of $x_f(t)$ and $\bar{x}_f(t)$, $P_f(t) = \langle x_f(t)x_f(t)^T\rangle$ and $\bar{P}_f(t) = \langle \bar{x}_f(t)\bar{x}_f(t)^T\rangle$, respectively. Finally, for $t > t_b$ (where t_b is the time needed for $P_f(t)$ and $\bar{P}_f(t)$ to converge to their steady-state values, and $t_b \to 0$ as $\varepsilon \to 0$), $P_f(t)$ and $\bar{P}_f(t)$ converge to $P_f(\infty)$ and $\bar{P}_f(\infty)$, respectively (both $P_f(\infty)$ and $\bar{P}_f(\infty)$ are bounded quantities, which follows from closed-loop stability). Because $\mathcal{A}_{f\varepsilon}$ is a diagonal matrix, the trace of matrix $\bar{P}_f$ can be computed as follows[18]

$$Tr\{\bar{P}_f\} = \frac{\varepsilon}{2} \cdot \sum_{i=1}^{\infty} \left|\frac{1}{\lambda_{\varepsilon i}}\right| \tag{34}$$

where $\lambda_{\varepsilon i}$ ($i = 1, 2, \ldots, \infty$) are the eigenvalues of the matrix $\mathcal{A}_{f\varepsilon}$ in Eq. 31. According to Assumption 1, $\sum_{i=1}^{\infty} |\frac{1}{\lambda_{\varepsilon i}}|$ converges to a finite positive number, and, thus, there exists a positive real number $k_{f\varepsilon}$ such that

$$Tr\{\bar{P}_f\} < \frac{\varepsilon}{2} \cdot k_{f\varepsilon} \tag{35}$$

Therefore, it follows that

$$Tr\{\bar{P}_f\} = \|var(\bar{x}_f)\|^2 = O(\varepsilon) \tag{36}$$

According to Eq. 33, it follows that the $\|var(x_f)\|^2$ is $O(\varepsilon)$. This completes the proof of Eq. 25 in Theorem 1. □

Proof of Eq. 26 in Theorem 1. Consider the x_s subsystem of the closed-loop system of Eq. 24. First, we note that there exists a positive real number k_{1s} such that[34,35]

$$\|\mathcal{F}_s(x_s, x_f) - \mathcal{F}_s(x_s, 0)\| < k_{1s}\|x_f\| \tag{37}$$

where the definition of the vector norm can be found in Eq. 13. From Eq. 32, we have the following estimate for $\|x_f\|$ for $t \ge t_b$ (where t_b is the time needed for $\|\bar{x}_f(t)\|$ to approach zero, and $t_b \to 0$ as $\varepsilon \to 0$):

$$\|x_f(t)\| = O(\sqrt{\varepsilon}) \tag{38}$$

This implies that we have the following estimate for $\|\mathcal{F}_s(x_s, x_f) - \mathcal{F}_s(x_s, 0)\|$ for $t \ge t_b$

$$\|\mathcal{F}_s(x_s, x_f) - \mathcal{F}_s(x_s, 0)\| = O(\sqrt{\varepsilon}) \tag{39}$$

Therefore, the solution of the following system consists an $O(\sqrt{\varepsilon})$ approximation of the x_s of Eq. 24[42], (Kokotovic, Khalil, and O'Reilly, Academic Press, 1986) Theorem A.1, p. 361.

$$\frac{d\bar{x}_s}{dt} = \mathcal{A}_{cs}\bar{x}_s + \xi_s \tag{40}$$

In particular, there exists an $\hat{\varepsilon}^{**} > 0$, such that for all $\varepsilon \in (0, \hat{\varepsilon}^{**}]$, it holds that

$$x_s(t) - \bar{x}_s(t) = O(\sqrt{\varepsilon}) \tag{41}$$

and

$$\begin{aligned}&\|var(x_s(t))\|^2 - \|var(\bar{x}_s(t))\|^2 = \left\langle \|x_s(t)\|^2 - \|\bar{x}_s(t)\|^2 \right\rangle \\ &\quad = \langle (\|x_s(t)\| - \|\bar{x}_s(t)\|) \cdot (\|x_s(t)\| + \|\bar{x}_s(t)\|) = O(\sqrt{\varepsilon})\end{aligned} \tag{42}$$

Note that it is assumed that the controller of Eqs. 19 and 21 can successfully drive the norm of the variance of x_s of the system of Eq. 20 to track the reference trajectory, which means the following equation holds

$$\|var(\bar{x}_s(t))\|^2 = \|var(x_s^*(t))\|^2 \tag{43}$$

Based on Eqs. 42 and 43, we immediately have that in the closed-loop infinite-dimensional system of Eq. 24, the following holds

$$\|var(x_s(t))\|^2 = \|var(x_s^*(t))\|^2 + O(\sqrt{\varepsilon}) \tag{44}$$

This completes the proof of Eq. 26 in Theorem 1. □

Proof of Eq. 27 in Theorem 1. According to Eq. 14, we have the following equation for $\|var(x(t))\|^2$ in Eq. 24

$$\|var(X(t))\|^2 = \|var(x_s(t))\|^2 + \|var(x_f(t))\|^2 \tag{45}$$

Using Eqs. 25 and 26, we have

$$\|var(X(t))\|^2 = \|var(x_s^*(t))\|^2 + O(\sqrt{\varepsilon}) + O(\varepsilon) \tag{46}$$

Since as $\varepsilon \to 0$, it holds that

$$\frac{O(\varepsilon)}{O(\sqrt{\varepsilon})} \to 0 \tag{47}$$

The $O(\varepsilon)$ term in Eq. 46 is very small relative to the term $O(\sqrt{\varepsilon})$ and can be neglected. Thus, there exists an $\varepsilon^* = min(\hat{\varepsilon}^*, \hat{\varepsilon}^{**})$ such that if $\varepsilon \in (0, \varepsilon^*]$, then

$$\|var(X(t))\|^2 = \|var(x_s^*(t))\|^2 + O(\sqrt{\varepsilon}) \tag{48}$$

This completes the proof of Theorem 1. ■

Simulation Results

In this section, we present applications of the proposed model predictive controller to both the stochastic PDE model and the kinetic Monte Carlo model of a sputtering process. Since the physical interpretation of the state variance of a stochastic PDE is the expected roughness of the surface modeled by the stochastic PDE, we will use the expected surface roughness as the control objective in the simulation study. By applying the MPC to the stochastic KSE, we demonstrate that the nonlinear MPC is able to regulate the expected surface roughness of the process modeled by the stochastic KSE to a desired level, and the proposed predictive controller possesses good robustness properties against model uncertainties. To demonstrate the applicability of the proposed predictive control method to control surfaces directly formed by microscopic events, we also apply the predictive controller to the kinetic Monte Carlo model of a sputtering process to demonstrate that the controller designed based on the stochastic KSE model of the process can regulate the surface roughness of the kinetic Monte Carlo model of the same process to a desired level.

Nonlinear predictive control of the stochastic Kuramoto-Sivashinsky equation

In this section, we present applications of the proposed predictive controller to a stochastic KSE. The stochastic KSE is a fourth-order nonlinear stochastic partial differential equation that describes the evolution of the height fluctuation for surfaces in a variety of material preparation processes, including surface erosion by ion sputtering,[16,17] and surface smoothing by energetic clusters.[43] We consider the following stochastic KSE with spatially distributed control

$$\frac{\partial h}{\partial t} = -\nu\frac{\partial^2 h}{\partial x^2} - \kappa\frac{\partial^4 h}{\partial x^4} + \frac{\lambda}{2}\left(\frac{\partial h}{\partial x}\right)^2 + \sum_{i=1}^{p} \hat{b}_i(x)u_i(t) + \xi'(x,t) \tag{49}$$

where u_i is the i^{th} manipulated input, p is the number of manipulated inputs, $\hat{b}_i$ is the i^{th} actuator distribution function (i.e., $\hat{b}_i$ determines how the control action computed by the i^{th} control actuator, u_i, is distributed (e.g., point or distributed actuation) in the spatial interval $[-\pi, \pi]$), $\nu = 1.975 \times 10^{-4}$, $\kappa = 1.58 \times 10^{-4}$, $\lambda = 1.975 \times 10^{-4}$, $x \in [-\pi, \pi]$ is the spatial coordinate t is the time, $h(x,t)$ is the height of the surface at position x and time t and $\xi'(x,t)$ is a Gaussian white noise with zero mean and unit covariance

$$\langle \xi'(x,t)\xi'(x',t')\rangle = \delta(x-x')\delta(t-t'). \tag{50}$$

Equation 49 is subjected to periodic boundary conditions

$$\frac{\delta^j h}{\delta x^j}(-\pi,t) = \frac{\delta^j h}{\delta x^j}(\pi,t), \quad j = 0,\ldots,3 \tag{51}$$

and the initial condition $h(x, 0) = 0$. The parameters of the KSE are selected such that $\kappa < \nu$ so that there is one positive eigenvalue of the linear operator, and the zero solution of the open-loop system is unstable. Note that although a uniform initial condition is used in this simulation, nonuniform initial conditions can be handled by the MPC formulation proposed in this work in the same way. A 200*th* order stochastic ODE of Eq. 49 obtained via Galerkin's method is used to simulate the process (the use of higher-order approximations led to identical numerical results, thereby implying that the following simulation runs are independent of the discretization). The Dirac delta function involved in the covariance of ξ_α^n and ξ_β^n is approximated by $\frac{1}{\Delta t}$, where Δt is the integration time step.

Eigenvalue problem

To study the dynamics of Eq. 49, we initially consider the eigenvalue problem of the linear operator of Eq. 49, which takes the form

$$\begin{aligned} A\bar{\phi}_n(x) &= -\nu\frac{d^2\bar{\phi}_n(x)}{dx^2} - \kappa\frac{d^4\bar{\phi}_n(x)}{dx^4} = \lambda_n\bar{\phi}_n(x) \\ \frac{d^j\bar{\phi}_n}{dx^j}(-\pi) &= \frac{d^j\bar{\phi}_n}{dx^j}(+\pi); \quad j = 0,\ldots,3; \quad n = 1,\ldots,\infty \end{aligned} \tag{52}$$

where λ_n denotes an eigenvalue and $\bar{\phi}_n$ denotes an eigenfunction. A direct computation of the solution of the a forementioned eigenvalue problem yields $\lambda_0 = 0$ with $\psi_0 = 1/\sqrt{2\pi}$, and $\lambda_n = \nu n^2 - \kappa n^4$ (λ_n is an eigenvalue of multiplicity two) with eigenfunction $\phi_n = (1/\sqrt{\pi})\ \sin(nx)$ and $\psi_n = (1/\sqrt{\pi})\ \cos(nx)$ for $n = 1, \ldots, \infty$. Note that the $\bar{\phi}_n$ in Eq. 52 denotes either ϕ_n or ψ_n. From the expression of the eigenvalues, it follows that for fixed values of $\nu > 0$ and $\kappa > 0$, the number of unstable eigenvalues of the operator A in Eq. 52 is finite, and the distance between two consecutive eigenvalues (i.e., λ_n and λ_{n+1}) increases as n increases.

We then derive nonlinear stochastic ODE formulations of Eq. 49 using Galerkin's method. By substituting the expansion of $h(x,t)$ in terms of the eigenfunctions into Eq. 49, and taking the inner product with the adjoint eigenfunctions, the following system of infinite nonlinear stochastic ODEs is obtained

$$\begin{aligned} \frac{d\alpha_n}{dt} &= (\nu n^2 - \kappa n^4)\alpha_n + f_{n\alpha} + \sum_{i=1}^{p} b_{i\alpha_n}u_i(t) + \xi_\alpha^n(t) \\ \frac{d\beta_n}{dt} &= (\nu n^2 - \kappa n^4)\beta_n + f_{n\beta} + \sum_{i=1}^{p} b_{i\beta_n}u_i(t) + \xi_\beta^n(t) \end{aligned} \qquad n = 1,\cdots,\infty \tag{53}$$

The control objective is the expected value of the surface roughness r, which is modeled by the stochastic KSE and is represented by the standard deviation of the surface from its average height and is computed as follows

$$\left\langle r(t)^2 \right\rangle = \left\langle \frac{1}{2\pi}\int_{-\pi}^{\pi} [h(x,t) - \bar{h}(t)]^2 dx \right\rangle \tag{54}$$

where $\bar{h}(t) = \frac{1}{2\pi}\int_{-\pi}^{\pi} h(x,t)dx$ is the average surface height. The expected surface roughness $\langle r(t)^2\rangle$ can be rewritten in terms of $\alpha_n(t)$ and $\beta_n(t)$ as follows

$$\left\langle r(t)^2\right\rangle = \frac{1}{2\pi}\left\langle \int_{-\pi}^{\pi} (h(x,t)-\bar{h}(t))^2 dx \right\rangle$$
$$= \frac{1}{2\pi}\left\langle \int_{-\pi}^{\pi} \left[\sum_{i=1}^{\infty}\alpha_i(t)\phi_i(x)+\sum_{i=0}^{\infty}\beta_i(t)\psi_i(x)-\beta_0(t)\psi_0\right]^2 dx \right\rangle$$
$$= \frac{1}{2\pi}\left\langle \int_{-\pi}^{\pi} \left[\sum_{i=1}^{\infty}\alpha_i(t)^2\phi_i(x)^2+\beta_i(t)^2\psi_i(x)^2\right] dx \right\rangle$$
$$= \frac{1}{2\pi}\left\langle \sum_{i=1}^{\infty}(\alpha_i(t)^2+\beta_i(t)^2)\right\rangle = \frac{1}{2\pi}\left\langle \sum_{i=1}^{\infty}\left[\left\langle \alpha_i(t)^2\right\rangle + \left\langle \beta_i(t)^2\right\rangle\right]\right\rangle \tag{55}$$

Therefore, the control problem of the expected surface roughness is equivalent to the state covariance control of the stochastic KSE. The proposed predictive control method can be applied to regulate the expected surface roughness.

Open-loop dynamics of the stochastic KSE

In the first simulation, we compute the expected value of open-loop surface roughness profile from the solution of the stochastic KSE of Eq. 49 by setting $u_i(t) = 0$ for $i = 1,\ldots,p$. For $\nu = 1.975 \times 10^{-4}$ and $\kappa = 1.58 \times 10^{-4}$, the stochastic KSE possesses one positive eigenvalue. Therefore, the zero solution of the open-loop system is unstable. Surface roughness profiles obtained from 100 independent simulation runs using the same parameters are averaged, and the resulting surface roughness profile is shown in Figure 1. The value of the open-loop surface roughness increases due to the open-loop instability of the zero solution. On the other hand, due to the existence of the nonlinear term, the open-loop surface roughness does not increase exponentially, but it is bounded.

Model reduction

Following the same way of model reduction of Eq. 9, we rewrite the system of Eq. 53 as follows

$$\begin{aligned}\frac{dx_s}{dt} &= \Lambda_s x_s + f_s(x_s,x_f) + B_s u + \xi_s \\ \frac{dx_f}{dt} &= \Lambda_f x_f + f_f(x_s,x_f) + B_f u + \xi_f\end{aligned} \tag{56}$$

where $x_s = [\alpha_1 \cdots \alpha_m\ \beta_1 \cdots \beta_m]^T$, $x_f = [\alpha_{m+1}\ \beta_{m+1} \cdots]^T$, $\Lambda_s = diag[\lambda_1 \cdots \lambda_m\ \lambda_1 \cdots \lambda_m]$, $\Lambda_f = diag[\lambda_{m+1}\ \lambda_{m+1}\ \lambda_{m+2}\ \lambda_{m+2} \cdots]$, $f_s(x_s, x_f) = [f_{1\alpha}(x_s,x_f) \cdots f_{m\alpha}(x_s,x_f)\ f_{1\beta}(x_s,x_f) \cdots f_{m\beta}(x_s,x_f)]^T$, $f_f(x_s,x_f) = [f_{m+1\alpha}(x_s,x_f)\ f_{m+1\beta}(x_s,x_f) \cdots]^T$, $u = [u_1 \cdots u_p]$, $\xi_s = [\xi_\alpha^1 \cdots \xi_\alpha^m\ \xi_\beta^1 \cdots \xi_\beta^m]$, and $\xi_f = [\xi_\alpha^{m+1}\ \xi_\beta^{m+1} \cdots]$

$$B_s = \begin{bmatrix} b_{1_{\alpha_1}} & \cdots & b_{p_{\alpha_1}} \\ \vdots & \ddots & \vdots \\ b_{1_{\alpha m}} & \cdots & b_{p_{\alpha m}} \\ b_{1_{\beta_1}} & \cdots & b_{p_{\beta_1}} \\ \vdots & \ddots & \vdots \\ b_{1_{\beta_m}} & \cdots & b_{p_{\beta_m}} \end{bmatrix} \quad B_f = \begin{bmatrix} b_{1_{\alpha_{m+1}}} & \cdots & b_{p_{\alpha_{m+1}}} \\ b_{1_{\alpha_{m+1}}} & \cdots & b_{p_{\beta_{m+1}}} \\ b_{1_{\alpha_{m+2}}} & \cdots & b_{p_{\alpha_{m+2}}} \\ b_{1_{\alpha_{m+2}}} & \cdots & b_{p_{\beta_{m+2}}} \\ \vdots & \vdots & \vdots \end{bmatrix} \tag{57}$$

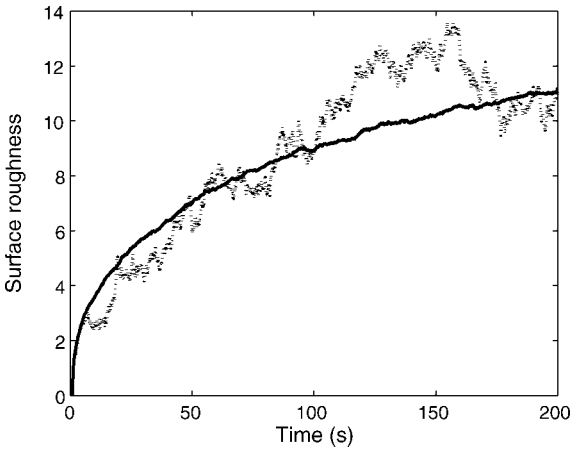

Figure 1. Comparison of the open-loop expected surface roughness profile computed by averaging 100 independent simulation runs (solid line) and that from a single simulation run (dotted line) of the stochastic KSE of Eq. 49.

We note that the subsystem x_f in Eq. 56 is infinite-dimensional. Neglecting the x_f subsystem, the following $2m$-dimensional system is obtained

$$\frac{d\tilde{x}_s}{dt} = \Lambda_s \tilde{x}_s + f_s(\tilde{x}_s, 0) + B_s u + \xi_s \tag{58}$$

where the tilde symbol in $\tilde{x}_s$ denotes that this state variable is associated with a finite-dimensional system.

Nonlinear predictive control of the stochastic KSE

In this closed-loop simulation, we design a predictive controller based on a $10th$-order stochastic ODE approximation constructed by using the first 10 eigenmodes of the system of Eq. 49. Ten control actuators are used to control the system. The ith actuator distribution function is taken to be:

$$b_i(z) = \begin{cases} \frac{1}{\sqrt{\pi}}\sin(iz); & i = 1,\ldots,5 \\ \frac{1}{\sqrt{\pi}}\cos[(i-5)z]; & i = 6,\ldots,10 \end{cases} \tag{59}$$

Under this control problem formulation, $m = 5$ and the value of $\varepsilon = |\lambda_1|/|\lambda_{11}| = 4.21 \times 10^{-4}$. Our desired expected value of the surface roughness in 4.28. A reference trajectory for the expected surface roughness is constructed and is shown by the dotted line in Figure 2. Closed-loop simulations are performed to study the evolution of the expected value of the surface roughness under predictive control. To further simplify the computation, the predictive controller is solved by assuming that all the closed-loop poles of the finite-dimensional system are equal to each other. Closed-loop surface roughness profiles obtained from 100 independent simulation runs using the same simulation parameters are averaged, and the resulting surface roughness profile is shown in Figure 2 (solid line), and it is compared with the reference trajectory (dotted line). We can see that the controller successfully drives the surface roughness to

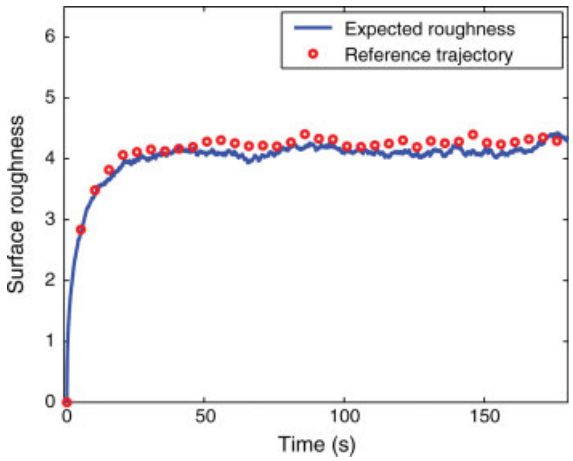

Figure 2. The closed-loop profile of the expected value of the surface roughness of the nonlinear KSE under predictive control (solid line) vs. the reference trajectory.

[Color figure can be viewed in the online issue, which is available at www.interscience.wiley.com.]

the desired level, which is lower than that corresponding to open-loop operation ($u_i(t) = 0$, $i = 1,\ldots,10$) shown in Figure 1.

Robustness properties of the predictive controller

In this subsection, we demonstrate the good robustness properties of the model predictive controller against parameter uncertainties of the stochastic KSE process model. To this end, we consider significant uncertainty in the parameters of the stochastic KSE process model. Specifically, the controller is designed based on the stochastic KSE model with the following parameters $\nu_m = 1.975 \times 10^{-4}$, $\kappa_m = 1.58 \times 10^{-4}$, and $\lambda_m = 1.975 \times 10^{-4}$, where the subscript m denotes that the parameter is used by the model predictive controller design. However, the parameters of the stochastic KSE to which the predictive controller is applied are, $\nu = 1.5\nu_m$, $\kappa = 0.5\kappa_m$, and $\lambda = 1.2\lambda_m$, which correspond to a 50% uncertainty associated with ν and κ and a 20% uncertainty associated with λ. Both the proposed predictive controller and the pole placement covariance controller proposed in our previous work[22] are applied to the stochastic KSE model with the model uncertainties, and the simulation results are shown in Figure 3. It is clear that the pole placement covariance controller developed in our previous work fails to regulate the expected surface roughness to the desired level, but the predictive controller successfully regulates the expected surface roughness to the desired level in the presence of significant model uncertainties.

Remark 2 *Note that in the pole placement covariance controller[22] the closed-loop poles are determined based on the stochastic KSE model and the desired expected surface roughness through an off-line design procedure. When there are model errors, the errors will propagate to the closed-loop poles of the controller, which results in a deteriorated closed-loop performance. In the proposed predictive controller, the closed-loop poles are computed by solving an online optimization problem. The online solution of the optimization problem provides a feedback mechanism, which compensates for the effect of model errors on the performance of the closed-loop system.*

Model predictive control of an ion-sputtering process described by the stochastic KSE

Sputtering processes are widely used in the thin film and semiconductor fabrication to remove material from the surface of solids through the impact of energetic particles.[31] In many cases sputtering is used to smooth out surface features. The stochastic KSE can be used to model the evolution of the height profile for surfaces in a variety of sputtering processes including surface erosion by ion sputtering,[16,17] and surface smoothing by energetic clusters.[43] Physical processes whose evolution of surface height can be modeled by the stochastic KSE can also be modeled by using kinetic Monte Carlo techniques (see, for example,[16,18]). Since kinetic Monte Carlo models predict the evolution of surface roughness in

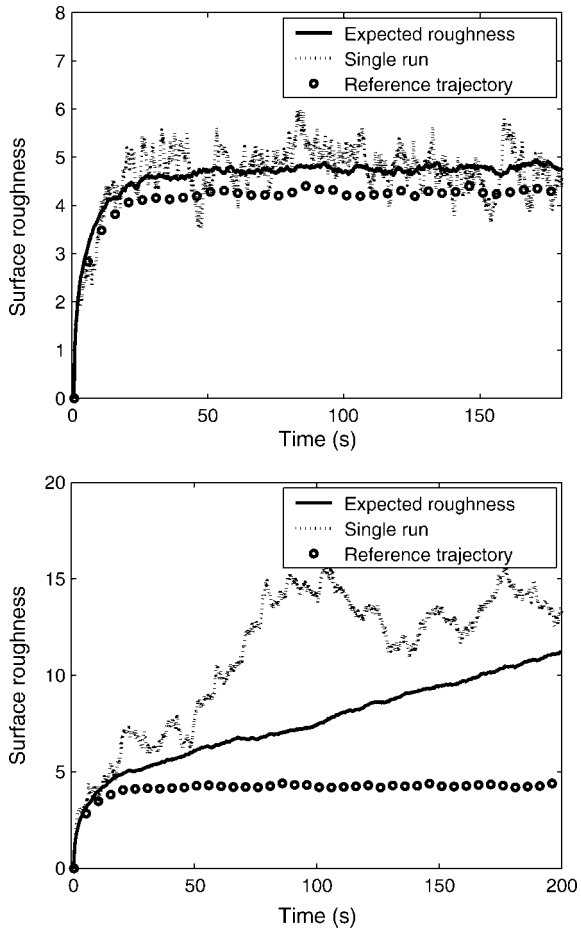

Figure 3. Comparison of the expected closed-loop surface roughness of the nonlinear KSE under the proposed predictive controller (top figure), and under the nonlinear pole placement controller developed in[22] (bottom figure): effect of model uncertainty.

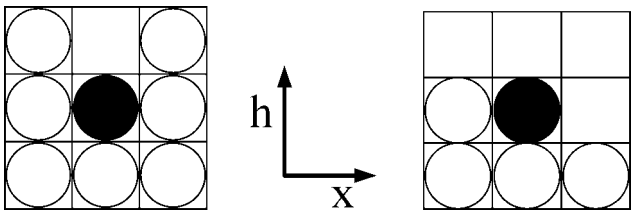

Figure 4. The rule to determine P_e.

P_e is defined as $\frac{1}{7}$ times the number of occupied sites in a box of size 3×3 centered at the particle on the top of site i; $P_e = 1$ in the left figure, and $P_e = \frac{4}{7}$ in the right figure, where the particle marked by ● is on the top of site i.

these processes by directly simulating the formation of the surface under various surface microprocesses, such as adsorption, desorption, surface erosion and surface reaction, kinetic Monte Carlo models have a higher accuracy for prediction of the surface roughness than the stochastic KSE model. To better verify the efficiency of the developed feedback controller, we implement the proposed nonlinear prodictive controller to the kinetic Monte Carlo process model of a sputtering process[16] to control the surface roughness to a desired level.

Process description

We consider a 1-D-lattice representation of a crystalline surface in a sputtering process, which includes two surface microprocesses, erosion and diffusion. The solid-on-solid assumption is made, which means that no defects or overhangs are allowed in the process.[44] The microscopic rules are as follows: a site, i, is first randomly picked among the sites of the whole lattice, and the particle at the top of this site is subject to: (a) erosion with probability $0 < f < 1$, or (b) diffusion with probability $1 - f$.

If the particle at the top of site i is subject to erosion, the particle is removed from the site i with probability $P_e \cdot Y(\phi_i)$. P_e is determined as $\frac{1}{7}$ times the number of occupied sites in a box of size 3×3 centered at the site i, which is shown in Figure 4. There is a total of nine sites in the box. The central one is the particle to be considered for erosion (the one marked by ●). Among the remaining eight sites, the site above the central site of interest must be vacant since the central site is a surface site. Therefore, only seven of the eight sites can be occupied, and the maximum value of P_e is 1. $Y(\phi_i)$ is the sputtering yield function defined as follows

$$Y(\phi_i) = y_0 + y_1\phi_i^2 + y_2\phi_i^4 \tag{60}$$

where y_0, y_1 and y_2 are process dependent constants, and ϕ_i is the local slope defined as follows

$$\phi_i = \tan^{-1}\left(\frac{h_{i+1} - h_{i-1}}{2a}\right) \tag{61}$$

where a is the lattice parameter, and h_{i+1} and h_{i-1} are the values of surface height at sites $i + 1$ and $i-1$, respectively.

If the particle at the top of site i is subject to diffusion, one of its two nearest neighbors, j ($j = i + 1$ or $i - 1$) is randomly chosen, and the particle is moved to the nearest neighbor column with probability $w_{i\to j}$ as follows

$$w_{i\to j} = \frac{1}{1 + \exp\left(\beta\Delta H_{i\to j}\right)} \tag{62}$$

where $\Delta H_{i\to j}$ is the energy difference between the final and initial states of the move, $\beta = \frac{1}{k_B T}$ and H is defined through the Hamiltonian of an unrestricted solid-on-solid model as follows[44]

$$H = \left(\frac{J}{a^n}\right)\sum_{k=1}^{L}(h_k - h_{k+1})^n \tag{63}$$

where J is the bond energy, L is the total number of sites in the lattice, and n is a positive number. In the simulations presented in this paper, we use $n = 2$ and $\beta \cdot J = 2.0$.

Kinetic Monte Carlo simulation of the sputtering process

To carry out kMC simulations of this sputtering process, the rates of surface microprocesses should be computed.[45,46] The rates of both erosion and diffusion are site specific, and can be obtained based on the process description as follows

$$\begin{aligned} r_e(i) &= \frac{f}{\tau}\cdot P_e(i)\cdot Y(\phi_i) \\ r_d(i,j) &= \frac{1-f}{2\tau}\cdot w_{i\to j} \end{aligned} \quad ; i = 1, 2, \ldots, L \tag{64}$$

where $r_e(i)$ is the erosion rate at site i, and $r_d(i,j)$ is the rate at which a surface particle hops from site i to site j. For the sputtering process considered, only nearest heighbor hopping is allowed, so $j = i \pm 1$. $P_e(i)$ is determined by the box rule shown in Figure 4, $Y(\phi_i)$ is defined in Eqs. 60 and 61, $w_{i\to j}$ is defined in Eqs. 62 and 63, and τ is the time scale.[17] After the rates of surface microprocesses are determined, kMC simulations can be carried out using an appropriate algorithm.[47] Periodic boundary conditions (PBCs) are used in the kMC model of the sputtering process. Using PBCs, a particle that diffuses out of the simulation lattice at one boundary enters into the simulation lattice from the opposing side. Limited by the currently available computing power, the lattice size of a kMC simulation is much smaller than the size of a real process. Therefore, PBCs are widely used in molecular microscopic level simulations, so that the statistical properties of a large scale stochastic process can be appropriately captured by kMC simulations carried out on a small simulation lattice.[48]

Remark 3 *The stochastic PDE model and the kMC model of the sputtering process are consistent. The stochastic PDE model for the sputtering processes can be derived based on the corresponding master equation (see, for example,[17,49]). Mathematically, the kMC model is a first-principle realization of the microscopic process that provides an unbiased realization of the master equation. Therefore, the evolution of the surface configuration predicted by the closed-form stochastic PDE model is consistent to that predicted by the kMC model, and, thus, can be controlled by a controller designed, based on the stochastic PDE model of the same process.[18,19,21,22] However, the parameters of the*

stochastic KSE derived, based on the corresponding master equation need to be carefully estimated. A continuum limit is used in the derivation of the stochastic KSE from the master equation, which requires an infinite number of lattice sites in the kMC model. From a practical point of view, a kMC model with a finite number of lattice sites is, however, used for the simulation of the sputtering process, thereby leading to a mismatch between the stochastic KSE and the kMC model. Therefore, it is necessary to estimate the parameters of the stochastic KSE, based on the kMC data directly to ensure that the KSE model predictions are close to the ones of the kMC model. (See the following for parameter estimation.)

Necessity of spatially distributed control

Both spatially distributed control configuration[18,19,22] and spatially invariant control configuration[2,3,21] could be used to control the surface roughness of various material preparation processes. However, the selection of control configurations in the previous works was largely arbitrary, and was not guided by the characteristics of the specific process considered. In this section, we investigate the necessity and effectiveness of spatially distributed control configuration in the context of control of processes described by nonlinear stochastic PDEs.

For the ion-sputtering process considered in this section, we consider the manipulated input as either the surface bombardment rate or the substrate temperature. We will demonstrate through the kMC simulation of the sputtering process that a desired expected surface roughness value, 0.3, cannot be achieved by manipulating either the substrate temperature or the surface bombardment rate as a spatially invariant process input, but can be achieved by manipulating the surface bombardment rate as a spatially distributed process input.

In the first set of simulation runs, we compute the expected surface roughness profiles of the sputtering process during the erosion of the first 1,000 monolayers under different substrate temperature. In all simulation runs, $f = 0.5$ and $\beta \cdot J = J/k_BT$ changes from 0.05 to 5.0. Note that in each simulation run, the substrate temperature is spatially invariant

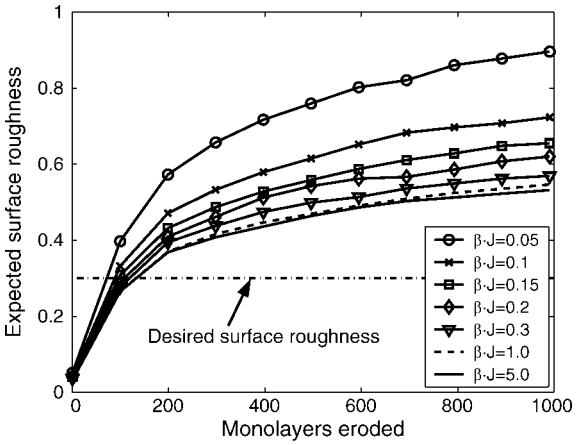

Figure 5. Comparison of the open-loop profile of the expected surface roughness from the kMC simulator when $f = 0.5$ and $\beta \cdot J$ varies from 0.05 to 5.0.

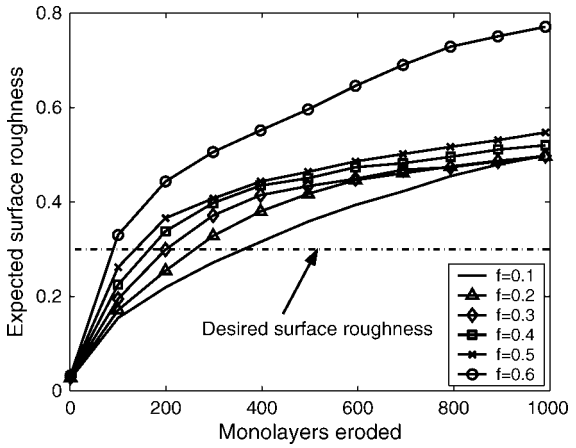

Figure 6. Comparison of the open-loop profile of the expected surface roughness from the kMC simulator when $\beta \cdot J = 2.0$ and f varies from 0.1 to 0.6.

and constant. The surface roughness is calculated as the standard deviation of the surface height profile. In the kMC simulation, the formula to compute the surface roughness is as follows

$$r = \sqrt{\frac{1}{L}\sum_{i=1}^{L}(h_i - \bar{h})^2} \tag{65}$$

where L denotes the number of the lattice sites on the lateral direction, and $\bar{h}$ denotes the averaged value of the surface height among all lattice sites. The expected surface roughness is the average of surface roughness profiles obtained from 100 independent runs.

Figure 5 shows a comparison of the expected surface roughness profiles under different temperatures. It is clear that although the expected surface roughness can be reduced by decreasing the temperature (or increasing the value of $\beta \cdot J$), the reduction is quite limited. Furthermore, it can be observed that the minimum expected surface roughness that can be achieved by manipulating the substrate temperature as a spatially invariant process input is around 0.5, which is much higher than the desired surface roughness of 0.3 in this case study.

In the second set of simulation runs, we compute the expected surface roughness profiles of the sputtering process during the erosion of the first 1,000 monolayers under different values of the erosion probability f. In all simulation runs, the substrate temperature is fixed such that $\beta \cdot J = 2.0$ and the probability that a selected surface particle is subjected to erosion f, changes from 0.1 to 0.6. Note that in each simulation run, the value of f is fixed. The erosion probability can be changed by varying the surface bombardment rate.[47] In this study, the change of f from 0.1 to 0.6 corresponds to the change of surface bombardment rate from $0.1 sec^{-1}\ site^{-1}$ to $1.5 sec^{-1} site^{-1}$.

Figure 6 shows the comparison of the expected surface roughness profiles under different values of f. Again, although the expected surface roughness can be reduced by

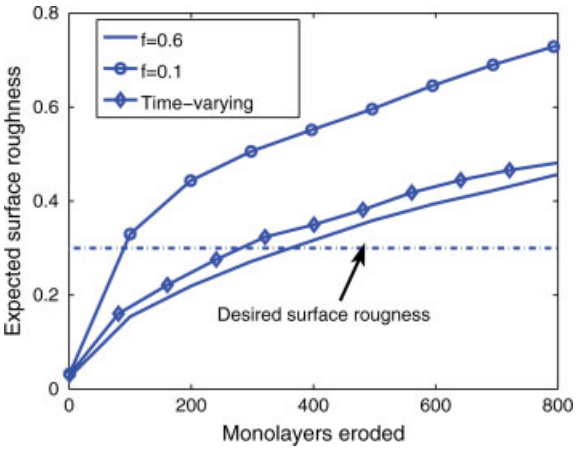

Figure 7. Comparison of open-loop profiles of the expected surface roughness from the kMC simulator when $\beta \cdot J = 2.0$ and f is (1) f = 0.6, (2) f = 0.1, and (3) time-varying.

[Color figure can be viewed in the online issue, which is available at www.interscience.wiley.com.]

decreasing the value of f, the reduction is quite limited. It can be observed that the minimum expected surface roughness that can be achieved by manipulating the surface bombardment rate as a spatially invariant process input is around 0.5, which is higher than the desired surface roughness of 0.3 in this case study.

Finally, we consider a case where f is spatially invariant, but is time-varying. Specifically, for each monolayer eroded, $f = 0.1$ for the first half monolayer, and $f = 0.6$ for another half monolayer. We compute the expected surface roughness profiles of the sputtering process during the erosion of the first 800 monolayers under this time-varying erosion probability f. In all simulation runs, the substrate temperature is fixed such that $\beta \cdot J = 2.0$. Figure 7 shows the profile of the expected surface roughness under this operation. The profile is also compared to those under fixed values of f ($f = 0.1$ and $f = 0.6$). It can be observed that when f is time-varying between 0.1 and 0.6, the resulted expected surface roughness profile is between the profiles obtained under fixed values of $f = 0.1$ and $f = 0.6$. Although time-varying inputs are useful for surface processing in certain applications, they are not effective in reducing the surface roughness of the sputtering process considered in this work. The surface roughness obtained from this time-varying input is around 0.5, and is also higher than the desired surface roughness of 0.3.

Based on the simulation results shown in this section, it can be concluded that reduction of the expected surface roughness of the sputtering process by manipulation either of the substrate temperature or of the surface bombardment rate as a spatially invariant process input is very limited, and, in the case studies, the desired surface roughness which is 0.3, cannot be achieved. In the following subsection, we will demonstrate that this limitation can be overcome by the proposed nonlinear controller designed based on the stochastic KSE process model, which uses spatially distributed control actuation. To this end, we consider a sputtering process with fixed substrate temperature ($\beta \cdot J = 2.0$), and control the expected surface roughness to the desired value by manipulating the spatially distributed surface bombardment rate across the surface.

Remark 4 *Note that in this work, we focus on the predictive control of surface roughness in processes that can be modeled by nonlinear stochastic PDEs so that a prespecified surface roughness can be achieved. For a specific material preparation process, the desired surface roughness should be determined based on the process characteristics and the product specifications. Detailed discussion on the selection of desired surface roughness for a variety of existing thin film deposition and sputtering processes is beyond the scope of this work.*

Stochastic KSE model with spatially distributed control

In the remainder of this section, a stochastic KSE model will be identified using surface snapshots generated by the kMC simulation of the sputtering process, and the spatially distributed control action will be computed using the proposed model predictive controller designed on the basis of the identified stochastic KSE model.

The equation for the height fluctuations of the surface in this sputtering process was derived in[17] and is a stochastic Kuramoto-Sivashinsky equation of the form of Eq. 66

$$\frac{\partial h}{\partial t} = -\nu\frac{\partial^2 h}{\partial x^2} - k\frac{\partial^4 h}{\partial x^4} + \frac{\lambda}{2}\left(\frac{\partial h}{\partial x}\right)^2 + \xi(x,t) \qquad (66)$$

where $x \in [-\pi, \pi]$ is the spatial coordinate, t is the time, $h(x\ t)$ is the height of the surface at position x and time t, and $\xi(x, t)$ is a Gaussian noise with zero mean and covariance

$$\langle \xi(x,t)\xi(x',t')\rangle = \sigma^2\delta(x-x')\delta(t-t') \qquad (67)$$

where σ is a constant. We note that this stochastic KSE representation for the surface morphological evolution in sputtering processes is limited to surface morphologies that do not involve re-entrant features; the re-entrant features could arise under certain sputtering conditions, and are catastrophic for the surface.

Parameter estimation

While the parameters of stochastic PDE models for many deposition and sputtering processes can be derived based on the corresponding master equation, which describe the evolution of the probability that the surface is at a certain configuration; for all practical purposes, the stochastic PDE model parameters should be estimated by matching the prediction of the stochastic PDE model to that of kMC simulations, due to the approximations made in the derivation of the stochastic PDE model from the master equation.[18,50]

A method was recently developed to estimate the parameters of the nonlinear stochastic KSE model of the sputtering process by using data from the kMC simulations of the process.[47] The parameter estimation algorithm is developed on the basis of the finite-dimensional model, which takes the

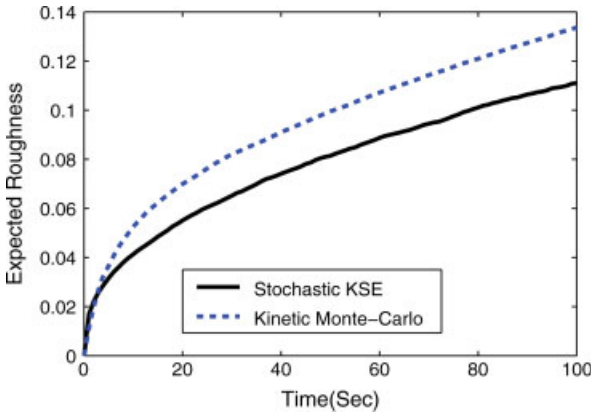

Figure 8. Comparison of the open-loop profile of the expected surface roughness of the sputtering process from the kMC simulator and that from the solution of the stochastic KSE using the estimated parameters.

[Color figure can be viewed in the online issue, which is available at www.interscience.wiley.com.]

form of Eq. 58. The derivation of the finite-dimensional approximation of the stochastic KSE model (Eq. 66) of the sputtering process follows the same method as described in the model reduction of the MPC design previously. The system of Eq. 58 is a finite-dimensional nonlinear stochastic ODE system including all four model parameters, ν, κ, λ, and σ^2 of the stochastic KSE of Eq. 66. A system of deterministic ODEs is then derived to describe the dynamics of the state covariance matrix. The diagonal elements of the deterministic ODE system are used to estimate the four parameters. Profiles of the state covariance are obtained by averaging the results from kMC simulations. Finally, the model parameters of the stochastic KSE of Eq. 66 are estimated by using the least-square fitting method.

The method was applied to the ion-sputtering process to identify the parameters of the stochastic KSE model with the first $2m = 20$ modes for parameter estimation. To formulate the least-squares fitting problem, the state covariances were evaluated at the first 150 available discrete time instants in the data obtained from kMC simulations. The values of the four parameters obtained from least-squares fitting are $\nu = 2.76 \times 10^{-5}$, $\kappa = 1.54 \times 10^{-7}$, $\lambda = 3.06 \times 10^{-3}$, and $\sigma^2 = 1.78 \times 10^{-5}$.

To validate the parameter estimation method, the expected open-loop surface roughness was computed from the stochastic KSE model of Eq. 66 with the computed parameters. Then, the profile from the stochastic KSE with computed parameters was compared to that from the kMC model. The expected surface roughness was computed from the simulations of the stochastic KSE, and the kMC model by averaging surface roughness profiles obtained from 100 and 10,000 independent runs, respectively. The simulation result is shown in Figure 8. It is clear that the computed model parameters result in consistent expected surface roughness profiles from the stochastic KSE model of Eq. 66, and from the kMC simulator of the sputtering process. There is observable difference between the two profiles, which indicates the existence of a slight mismatch of the identified KSE model with the kMC model of the sputtering process. However, the error is compensated in the closed-loop MPC implementation through feedback since the MPC regulates the surface roughness of the kMC model at the desired level.

Model predictive control with distributed control action

In the closed-loop simulation, we design a predictive controller based on a 20th-order stochastic ODE approximation constructed by using the first 20 eigenmodes of the linearized (around zero solution) stochastic PDE of Eq. 66. First we design a linear state feedback controller as follows

$$u(t) \quad = \quad B_s^{-1}\{(A_{cs}(t) - A_s)\tilde{x}_s(t)\} \tag{68}$$

where $\mathcal{A}_{cs}(t) = diag[\lambda_{c1}(t) \cdots \lambda_{cm}(t)], \lambda_{ci}(t), i = 1, 2, \cdots, m,$ are time-varying, desired poles of the closed-loop finite-dimensional system and the poles $\lambda_{ci}(t)$ are computed by solving the following optimization problem:

$$\begin{aligned} \min_{A_{cs(t)}} \quad & \int_t^{t+T_p} \Big(Q||var(x_s(T)) - var(x_s^*(\tau))||^2\Big)d\tau \\ & + Q_f||var(x_s(t+Tp)) - var(x_s^*(t+T_p))||^2 \\ s.t. \quad & \\ & \frac{dx_s}{dt} = A_{cs}(t)x_s + \xi_s \\ & a_i < \lambda_i < b_i < 0; \quad i = 1, 2, \cdots, m. \end{aligned} \tag{69}$$

20 control actuators are used to control the system. The ith actuator distribution function is taken to be

$$b_i(z) = \begin{cases} \frac{1}{\sqrt{\pi}}\sin(iz); & i = 1, \cdots, 10 \\ \frac{1}{\sqrt{\pi}}\cos[(i-10)z]; & i = 11, \cdots, 20 \end{cases} \tag{70}$$

Under this control problem formulation, $m = 10$, and the value of $\varepsilon = |\lambda_1|/|\lambda_{21}| = 0.02$. Our desired expected value of the surface roughness is 0.3. To further simplify the computation, the predictive controller is solved by assuming that all the closed-loop poles of the finite-dimensional system are equal to each other. Note that the predictive controller of Eqs. 68–69 is the linearization around the zero solution of the predictive controller of Eqs. 19–21.

Then, we apply the designed predictive controller to the kMC model of the sputtering process to control the surface roughness to the desired level. In this simulation, the initial surface roughness is about 0.5, and the microstructure of the initial surface is shown in Figure 9. The controller is implemented by manipulating the probability that a randomly selected site is subject to erosion rule f. Specifically, the f of site i is determined according to the following expression

$$f(i) = \frac{\bar{f} + \left(\sum_{j=1}^{20} b_j(z_i)u_j(t)\right)/a}{1 + \left(\sum_{j=1}^{20} b_j(z_i)u_j(t)\right)/a} \tag{71}$$

The following simulation algorithm is used to run the kinetic Monte Carlo simulations for the closed-loop system. First, a random number, ζ_1 is generated to pick a site i,

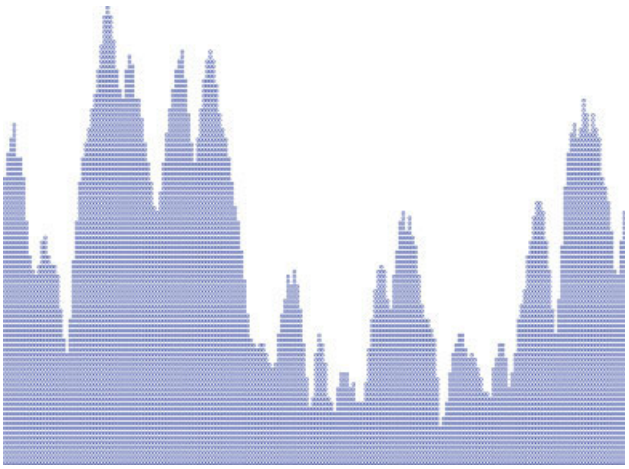

Figure 9. Surface microconfiguration at the beginning of the closed-loop simulation run: the initial surface roughness is 0.5.

[Color figure can be viewed in the online issue, which is available at www.interscience.wiley.com.]

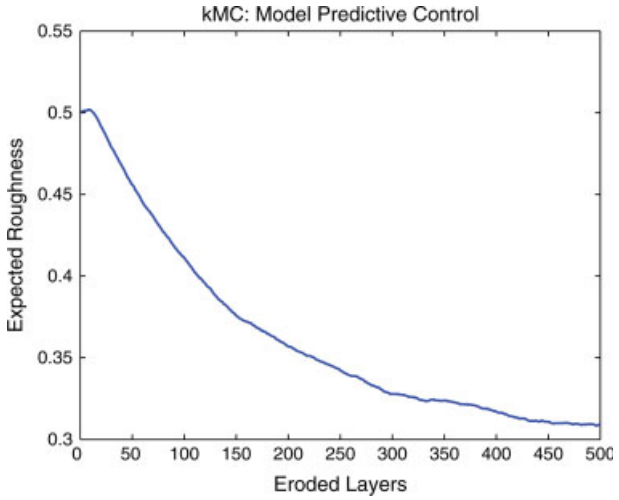

Figure 10. Closed-loop profile of the expected value of the surface roughness under predictive control.

[Color figure can be viewed in the online issue, which is available at www.interscience.wiley.com.]

among all the sites on the 1-D lattice; the probability that a surface site is subject to the erosion rules, $f(i)$ is determined by using Eq. 71. Then, the second random number, ζ_2 distributed uniformly in the (0, 1) interval is generated. If $\zeta_2 < f(i)$, the site i is subject to erosion, otherwise, the site is subject to diffusion.

If the site i is subject to erosion, P_e is computed by using the box rule shown in Figure 4, with the box centering at the surface particle on site i and $Y(\phi_i)$ is computed by using Eq. 60. Then, another random number, ζ_{e3} distributed uniformly in the (0, 1) interval is generated. If $\zeta_{e3} < P_e \cdot Y(\phi_i)$ the surface particle on site i is removed. Otherwise, no Monte Carlo event is executed.

If the site i is subject to diffusion, a side-neighbor, $j = i + 1$ or $i - 1$ is randomly picked, and the probability of a hopping from site i to site j, $w_{i\to j}$ is computed based on Eq. 62. Then, another random number ζ_{d3} distributed uniformly in the (0, 1) interval is generated. If $\zeta_{e3} < w_{i\to j}$, the surface particle on site i is moved to site j. Otherwise, no Monte Carlo event is executed. Once a Monte Carlo event is executed, the first 20 states ($\alpha_1, \ldots, \alpha_{10}$ and $\beta_1, \ldots, \beta_{10}$) are updated and new control actions are computed to update the value of f (defined in Eq. 71) for each surface site.

Closed-loop surface roughness profiles obtained from 100 independent simulation runs using the same simulation parameters are averaged, and the resulting expected surface roughness profile is shown in Figure 10. We can see that the predictive controller drives the surface roughness very close to the desired level, which is lower than the surface roughness that can be achieved by manipulating the surface bombardment rate in a spatially invariant manner.

The microstructure of the surface at the end of the closed-loop system simulation run is shown in Figure 11. It is clear that the proposed model predictive control results in a smoother closed-loop surface.

Remark 5 *Note that although the stochastic KSE model of Eq. 66 is a nonlinear model for the sputtering process, the linearization of the stochastic KSE around its zero solution is used to design the predictive controller of Eqs. 68–69. This is based on the following argument. Since the instability of the spatially uniform steady state comes from the linear part of the model, and the nonlinear part of the stochastic KSE helps bound the surface roughness, for control purposes, we only need to focus on the stabilization of the linear part of the stochastic KSE. This argument is further supported by our simulation results, which demonstrate the effectiveness of the predictive controller designed in this work.*

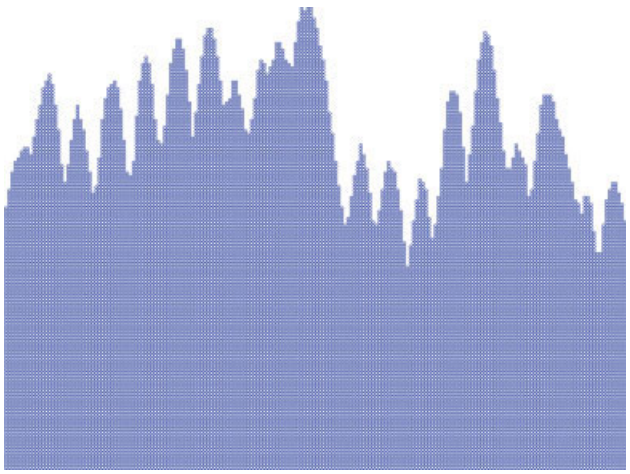

Figure 11. Surface microconfiguration at the end of the closed-loop simulation run under predictive control: the final surface roughness is around 0.3.

[Color figure can be viewed in the online issue, which is available at www.interscience.wiley.com.]

Conclusions

We developed a method for model predictive control of nonlinear stochastic PDEs to regulate the state variance to a desired level. Initially, a system of infinite nonlinear stochastic ODEs was derived from the nonlinear stochastic PDE by using Galerkin's method. To capture the dominant mode contribution, a finite-dimensional approximation of the stochastic ODE system was then derived. A model predictive control problem was formulated based on the approximation. This enabled computationally efficient prediction of state variance of the finite-dimensional system. The control action was computed by minimizing an objective penalty function. To characterize the closed-loop performance enforced by the model predictive controller, an analysis of the closed-loop nonlinear infinite-dimensional system was provided. The predictive controller was initially applied to the stochastic KSE, and resulted in successful control of the norm of the state variance to a desired level in the presence of significant model parameter uncertainties. In addition, the problem of surface roughness regulation in a 1-D ion-sputtering process including two surface microprocesses, diffusion and erosion, was considered. We established, through kMC simulations, that the spatially distributed control configuration was more effective for surface roughness regulation compared to the spatially invariant control configuration for this process. Then, we designed a model predictive controller based on an identified stochastic KSE surface model to control the surface roughness of the sputtering process by manipulating the surface bombardment rate in a spatially distributed manner. The predictive controller successfully regulated the expected surface roughness to a desired level in the kMC model of the sputtering process.

Acknowledgments

Financial support from NSF, CBET-0652131, is gratefully acknowledged by Gangshi Hu and Panagiotis D. Christofides.

Literature Cited

1. Christofides PD, Armaou A. Control and optimization of multiscale process systems. *Comp Chem Eng*. 2006;30:1670–1686.
2. Lou Y, Christofides PD. Estimation and control of surface roughness in thin film growth using kinetic Monte-Carlo models. *Chem Eng Sci*. 2003;58:3115–3129.
3. Lou Y, Christofides PD. Feedback control of growth rate and surface roughness in thin film growth. *AIChE J*. 2003;49:2099–2113.
4. Lou Y, Christofides PD. Feedback control of surface roughness of GaAs (001) thin films using kinetic Monte-Carlo models. *Comp Chem Eng*. 2004;29:225–241.
5. Ni D, Christofides PD. Dynamics and control of thin film surface microstructure in a complex deposition process. *Chem Eng Sci*. 2005;60:1603–1617.
6. Varshney A, Armaou A. Multiscale optimization using hybrid PDE/kMC process systems with application to thin film growth. *Chem Eng Sci*. 2005;60:6780–6794.
7. Siettos CI, Armaou A, Makeev AG, Kevrekidis IG. Microscopic/stochastic timesteppers and "coarse" control: a kMC example. *AIChE J*. 2003;49:1922–1926.
8. Armaou A, Siettos CI, Kevrekidis IG. Time-steppers and "coarse" control of distributed microscopic processes. *Int J Robust Nonlin Contr*. 2004;14:89–111.
9. Varshney A, Armaou A. Identification of macroscopic variables for low-order modeling of thin- film growth. *Ind Eng Chem Res*. 2006;45:8290–8298.
10. Gallivan MA, Murray RM. Reduction and identification methods for Markovian control systems, with application to thin film deposition. *Int J Robust Nonlin Contr*. 2004;14:113–132.
11. Rusli E, Drews TO, Ma DL, Alkire RC, Braatz RD. Robust nonlinear feedforward-feedback control of a coupled kinetic Monte Carlo-finite difference simulation. *J Proc Contr*. 2006;16:409–417.
12. Edwards SF, Wilkinson DR. The surface statistics of a granular aggregate. *Proc Royal Soc Lond Series A*. 1982;381:17–31.
13. Villain J. Continuum models of crystal growth from atomic beams with and without desorption. *J Phys I*. 1991;1:19–42.
14. Vvedensky DD, Zangwill A, Luse CN, Wilby MR. Stochastic equations of motion for epitaxial growth. *Phys Rev E*. 1993;48:852–862.
15. Chua ALS, Haselwandter CA, Baggio C, Vvedensky DD. Langevin equations for fluctuating surfaces. *Phys Rev E*. 2005;72:051103.
16. Cuerno R, Makse HA, Tomassone S, Harrington ST, Stanley HE. Stochastic model for surface erosion via ion sputtering: dynamical evolution from ripple morphology to rough morphology. *Phys Rev Letts*. 1995;75:4464–4467.
17. Lauritsen KB, Cuerno R, Makse HA. Noisy Kuramote-Sivashinsky equation for an erosion model. *Phys Rev E*. 1996;54:3577–3580.
18. Lou Y, Christofides PD. Feedback control of surface roughness in sputtering processes using the stochastic Kuramoto-Sivashinsky equation. *Comp Chem Eng*. 2005;29:741–759.
19. Lou Y, Christofides PD. Feedback control of surface roughness using stochastic PDEs. *AIChE J*. 2005;51:345–352.
20. Ni D, Christofides PD. Construction of stochastic PDEs for feedback control of surface roughness in thin film deposition. In *Proceedings of American Control Conference*, Portland, OR; 2005: 2540–2547.
21. Ni D, Christofides PD. Multivariable predictive control of thin film deposition using a stochastic PDE model. *Ind Eng Chem Res*. 2005;44:2416–2427.
22. Lou Y, Christofides PD. Nonlinear feedback control of surface roughness using a stochastic PDE: design and application to a sputtering process. *Ind Eng Chem Res*. 2006;45:7177–7189.
23. Garcia CE, Prett DM, Morari M. Model predictive control: theory and practices - A survey. *Automatica*. 1989;25:335–348.
24. Allgower F, Chen H. Nonlinear model predictive control schemes with guaranteed stability. In: *NATO ASI on Nonlinear Model Based Process Control*. Berber, R, Kravaris, C, eds.; Kluwer: Dordrecht, the Netherlands; 1998:465–494.
25. Rawlings JB. Tutotial: model predictive control technology. In *Proceedings of the American Control Conference*. San Diego, CA; 1999:662–676.
26. Scokaert PO, Mayne DQ, Rawlings JB. Suboptimal model predictive control (feasibility implies stability). *IEEE Trans on Automatic Control*. 1999;44:648–654.
27. Dubljevic S, Mhaskar P, El-Farra NH, Christofides PD. Predictive control of parabolic PDEs with state and control constraints. *Int J Robust Nonlin Contr*. 2006;16:749–772.
28. Dubljevic S, Christofides PD. Predictive control of parabolic PDEs with boundary control actuation. *Chem Eng Sci*. 2006;61:6239–6248.
29. Dubljevic S, Mhaskar P, El-Farra NH, Christofides PD. Predictive control of transport-reaction processes. *Comp Chem Eng*. 2005;29: 2335–2345.
30. Kardar M, Parisi G, Zhang YC. Dynamic scaling of growing interfaces. *Phys Rev Lett*. 1986;56:889–892.
31. Makeev MA, Cuerno R, Barabasi AL. Morphology of ion-sputtered surfaces. *Nuclear Instrum Methods Phys Res B*. 2002;197:185–227.
32. Hotz A, Skelton RE. Covariance control theory. *Int J Control*. 1987;46:13–32.
33. Bernstein DS, Haddad WM. Robust stability and performance analysis for linear dynamic systems. *IEEE Trans Autom Contr*. 1989;34: 751–758.
34. Christofides PD, Daoutidis P. Finite-dimensional control of parabolic PDE systems using approximate inertial manifolds. *J Math Anal Appl*. 1997;216:398–420.
35. Christofides PD. *Nonlinear and Robust Control of PDE Systems: Methods and Applications to Transport-Reaction Processes*. Boston: Birkhäuser; 2001.
36. Åström KJ. *Introduction to Stochastic Control Theory*. New York: Academic Press; 1970.

37. Armaou A, Christofides PD. Dynamic optimization of dissipative PDE systems using nonlinear order reduction. *Chem Eng Sci*. 2002; 57:5083–5114.
38. Astrid P. *Reduction of process simulation models: a proper orthogonal decomposition approach*. Eindhoven, The Netherland: Technische Universiteit; 2004.
39. Brent RP. *Algorithms for minimization without derivatives*. Englewood Cliffs, New Jersey: Prentice-Hall; 1973.
40. Lagarias JC, Reeds JA, Wright MH, Wright PE. Convergence properties of the Nelder-Mead simplex method in low dimensions. *SIAM J Optimiz*. 1998;9:112–147.
41. Skelton RE, Xu JH, Yasuda K. Minimal energy covariance control. *Intl J Control*. 1994;59:1567–1578.
42. Kokotovic PV, Khalil HK, O'Reilly J. *Singular perturbations in control: analysis and design*. London: Academic Press; 1986.
43. Insepov Z, Yamada I, Sosnowski M. Surface smoothing with energetic cluster beams. *J Vac Sci Technol A - Vac Surf Films*. 1997;15:981–984.
44. Siegert M, Plischke M. Solid-on-solid models of molecular-beam epitaxy. *Phys Rev E*. 1994;50:917–931.
45. Fichthorn KA, Weinberg WH. Theoretical foundations of dynamical Monte Carlo simulations. *J Chem Phys*. 1991;95:1090–1096.
46. Vlachos DG. Multiscale integration hybrid algorithms for homogeneous-heterogeneous reactors. *AIChE J*. 1997;43:3031–3041.
47. Hu G, Lou Y, Christofides PD. Model parameter estimation and feedback control of surface roughness in a sputtering process. *Chem Eng Sci*. 2008;63:1800–1816.
48. Makov G, Payne MC. Periodic boundary conditions in ab initio calculations. *Phys Rev B*. 1995;51:4014–4022.
49. Vvedensky DD. Edwards-Wilkinson equation from lattice transition rules. *Phys Rev E*. 2003;67:025102(R).
50. Haselwandter C, Vvedensky DD. Fluctuations in the lattice gas for Burgers' equation. *J Phys A: Math Gen*. 2002;35:L579–L584.

Manuscript received Dec. 8, 2007, and revision received Mar. 26, 2008.